研 究 論 文

Automatic Anatomical Labeling Method of Cerebral Arteries in MR-Angiography Data Set

Akihiro Takemura[1)*], Masayuki Suzuki[1)], Hajime Harauchi[2)] and Yusuke Okumura[3)]

[1)] *Division of Health Sciences, Graduate School of Medical Science, Kanazawa University*
[2)] *Kawasaki College of Allied Health Professions*
[3)] *Department of Radiology, Ishikawa Saiseikai Kanazawa Hospital,*

Research Code No.: 208.9
Key words: Anatomical labeling, Cerebral artery, 2D/3D registration, MRA, DSA

Abstract

To improve the accuracy and robustness of 2D/3D registration of digital subtraction angiography images and magnetic resonance angiography (MRA) data, we have developed an automatic method for anatomical labeling of the cerebral arteries in MRA data. The anatomical labeling method is a location-based method which segments an artery tree to branches and classifies the branches into labeled segments, i.e., internal carotid arteries (ICA), basilar artery (BA), middle cerebral arteries (MCA), A1 segments of the anterior cerebral artery (ACA(A1)), other segments of the anterior cerebral artery (ACA), posterior communication arteries (PcomA) and posterior cerebral arteries (PCA), according to their location. Arteries were extracted from MRA data for this labeling method by the region-growing technique. Fifteen cases were examined to evaluate the method accuracy. The number of correctly segmented voxels in each artery segment was determined, and the correct labeling percentage was calculated based on the total number of voxels of the artery. Mean percentages were as follows: ACA, 82.7%; Right (R-) ACA(A1), 47.1%; Left (L-) ACA(A1), 46.1%; R-MCA, 80.4%; L-MCA, 74.1%; R-PcomA, 0.0%; L-PcomA, 3.3%; R-PCA, 60.3%; L-PCA, 66.9%; R-ICA, 90.7%; L-ICA, 90.7%; BA, 89.9%; and total arteries, 84.1%. The ACA, MCA, ICA and BA were consistently identified correctly.

Received Oct.27, 2006; revision accepted Feb.2, 2007

* 金沢大学医学系研究科保健学専攻〔〒920-0942 石川県金沢市小立野5-11-80〕Division of Health Sciences, Graduate School of Medical Science, Kanazawa University 5-11-80 Kodatsuno, Kanazawa 920-0942 Japan
E-mail: at@mhs.mp.kanazawa-u.ac.jp

1. Introduction

Several authors have proposed two-dimensional (2D)/three-dimensional (3D) registration methods for volume data and fluorography images to aid clinical interventions. Some of the methods registered and superimposed preoperative computed tomography volume data onto intraoperative fluorographs to aid in recognizing 3D location of lamber vertebrae or a stent in aorta for surgeries[1-5]. The others register volume data onto a portal radiograph to assess patient setup errors in radiation therapy[6,7].

Methods have also been proposed for 2D/3D registration of the cerebral arteries in magnetic resonance angiography (MRA) data and digital subtraction angiography (DSA) images[8-14] and we have developed a 2D/3D registration method of cerebral arteries[15]. For proper registration in the methods, the corresponding arteries must be selected in the MRA and DSA. In these previous studies, identification and extraction of the arteries was performed manually.

An automatic anatomical labeling method of cerebral arteries in MRA would allow automatic extraction of the arteries of interest and more complete automation of 2D/3D registration methods. If arteries appearing in a DSA image are known, the same arteries in MRA can be chosen for registration automatically according to the anatomical labeling result. Also, such arteries are known if the kind of DSA images is known, e.g. internal carotid arteriography or vertebral arteriography and so on, because arteries enhanced in DSA images usually depend on the position of a catheter tip. Here, we refer to the anterior cerebral artery, middle cerebral artery, and internal carotid artery as arteries for internal carotid arteriography.

For these 2D/3D registration methods, we developed an anatomical labeling method for cerebral arteries in MRA. This anatomical labeling method divides the cerebral artery tree into segments, and labels the segments according to their location. In this paper, we describe the automatic anatomical labeling method and evaluate its accuracy.

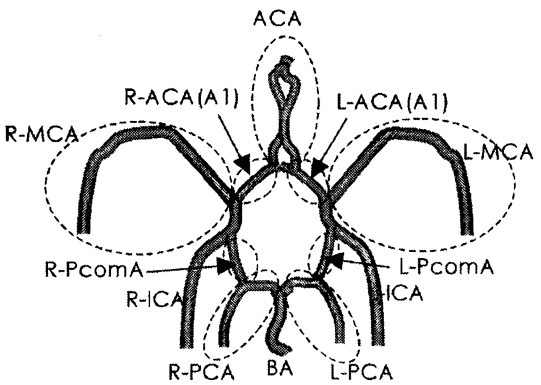

Fig. 1 Artery segments are classified into branches of the cerebral artery tree. The twelve segments are defined as follows: right (R-) and left (L-) internal carotid artery (ICA), basilar artery (BA), R- and L- middle cerebral artery (MCA), R- and L- posterior cerebral artery (PCA), R- and L- posterior communication artery (PcomA), R- and L- A1 segment of the anterior cerebral artery (ACA(A1)), and other segments of the anterior cerebral artery (ACA).

2. Materials and Methods

2.1. Anatomical Labeling Method

We developed a location-based anatomical labeling method that makes use of a 3D segment map of cerebral arteries. This method divides cerebral artery trees in MRA into twelve artery segments: right (R-) and left (L-) internal carotid artery (ICA), basilar artery (BA), R- and L- middle cerebral artery (MCA), R- and L- posterior cerebral artery (PCA), R- and L- posterior communication artery

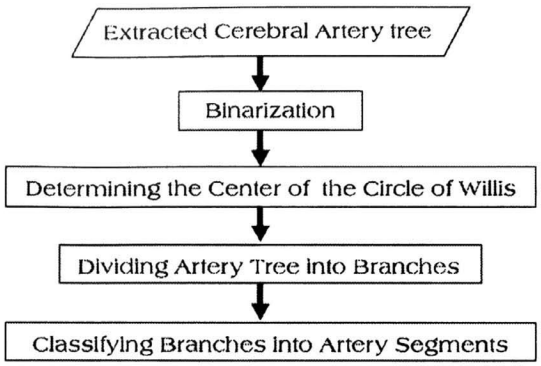

Fig. 2 Scheme of an anatomical labeling method for cerebral artery.

(PcomA), R- and L- A1 segment of the anterior cerebral artery (ACA(A1)) and other segments of the anterior cerebral artery (ACA) (Fig. 1). This division was selected to facilitate 2D/3D registration of a 2D DSA image and a 3D MRA data set. The scheme of this anatomical labeling method is shown in Fig. 2.

The anatomical labeling method we developed is given volume data of cerebral arteries extracted from MRA as input. Determination of the center of the circle of Willis (CW) is applied to suppress variation of CW positions between patients with 2D and 3D templates of CW. The cerebral arteries are divided into branches at bifurcations and each branch is labeled with one of the 12 artery segments using a 3D artery segment map. The segment map shows ranges of locations of each cerebral artery. Arteries of interest for 2D/3D registration can be extracted to specify the labels.

2.1.1. Extracted Cerebral Artery Trees

We used volume data of cerebral arteries extracted from MRA because there are many 2D/3D registration methods of cerebral artery target MRA data available. Many vessel extraction methods for MRA have been proposed[16-22]. The region-growing technique is generally used in such a segmentation method so that we used a simple region-growing technique to extract cerebral arteries from MRA volume data as a preliminary extraction method for this study. For the region-growing technique, a voxel is extracted if the mean value of that voxel and its six nearest neighbors is greater than a threshold value, and this is the only criterion for the technique. Voxel intensity in MRA usually depends upon both the patient and the magnetic resonance imaging system used, so several threshold values were applied for each case, and the lowest threshold value that resulted in no inclusion of the surrounding tissues was selected. In the future, we will improve the extraction process to do it automatically. Fig. 3 shows

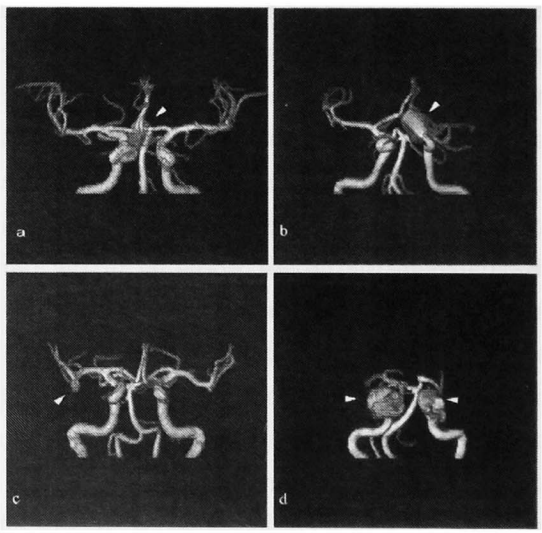

Fig. 3 Examples of the cerebral arteries extracted by the region-growing technique. These are volume rendered images of the anterior posterior view. The cases for the image (a), (b) and (d) have one or two giant aneurysms (white triangle) and the farther arteries did not appear in MRA. Thus, these arteries could not be extracted well. The case for image (c) also has an aneurysm on R-MCA.

examples of extracted cerebral artery trees. Extracted arteries were binarized.

2.1.2. Determining the Center of the Circle of Willis

There are slight positional differences between artery trees in MRAs. Although the patient's head is fixed in a head coil at the correct position, arteries in MRA volumes are not located in the same position in all patients according to morphological differences of the head, brain, arteries, etc. Thus, the positions of the arteries must be aligned prior to application of the location-based labeling method. We performed this registration using a two-step procedure to determine the 3D center of the CW as the origin. In the first step, the X and Y coordinates of the center of the CW are determined using a 2D template, which approximates a projection of the CW into the axial plane. For this 2D alignment, the binary artery tree is projected onto the XY plane and its location is varied to maximize the cross-correlation with the 2D template. With the X and Y coordinates of the center aligned, a 3D template approximating the CW is then used to determine the Z coordinate, by varying the Z coordinate of the 3D template and determining the maximum in the cross-correlation of the template and data. At the end of this registration, the X, Y and Z coordinates are again adjusted using Powell's optimization method[23]. Fig. 4 shows the 2D and 3D templates, which were based on preliminary measurements of the anterior communicating artery (AcomA), the R- and L- IC bifurcations (IC-Bif) and the top of the basilar artery (BA-top). Averaged coor-

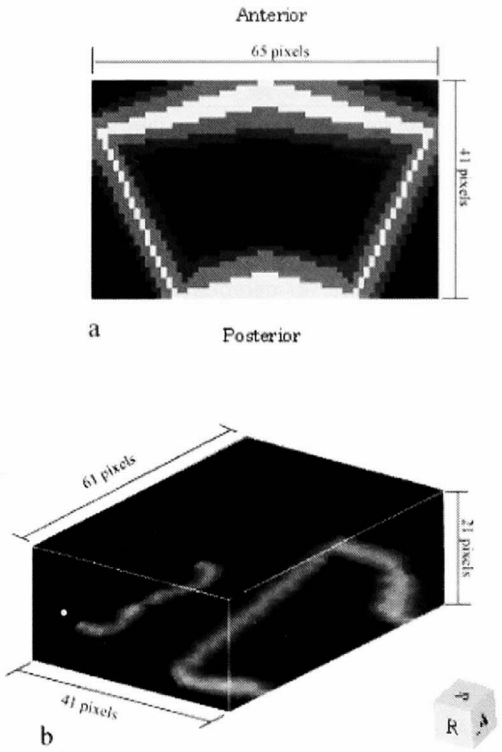

Fig. 4 2D and 3D templates of the Circle of Willis. Image (a) is the 2D template and image (b) is the volume rendered image of the 3D template. The highest voxel value is depicted by white; the lowest voxel value is depicted by black. The form in the 2D template is assimilated to a projection of the CW, and tubular structures in the 3D template are assumed parts of ACA, ICA and PCA on the CW. These templates were modelled from MRAs of five cases.

Table 1 The average coordinates of the anterior communicating artery (AcomA), the right (R-) and left (L-) internal carotid bifurcations (IC-Bif), and the top of the basilar artery (BA-top) originating with the midpoint between AcomA and BA-top.

	AcomA			R-IC-bif			L-IC-bif			BA-top		
	x	y	z	x	y	z	x	y	z	x	y	z
Averaged coordinates	0.8	−9.5	2.4	−28.4	−4.8	0.2	26.0	−5.6	−1.2	−0.8	19.0	−2.4
Standard deviation	1.1	1.3	2.6	8.0	3.9	4.5	5.9	2.2	5.3	2.2	2.7	2.6

(pixel)

dinates of the four points (Table 1) were calculated from five of the fifteen cases (see Section 2.3) with no aneurysms on the CW for these measurements.

We did not determine the rotation angles about the X-, Y- and Z-axes as the patient's head is placed in a head coil and is usually positioned in a standard manner. The angular misalignments should be small as MRI systems can take arbitrary oblique cross sections. In a preliminary study, we found that optimizations without the rotation parameters yielded better final results than those with these parameters, probably because the number of local maxima (incorrect alignments) increases with the number of parameters. The optimization searches the global maximum of the cross correlation values with varying parameters, but does not check all combinations of the parameters, so that, the optimization sometimes takes a local maximum of the value as the global maximum. Incrementation of the number of the parameters increases the number of their combinations; incrementation of the number of combinations increases the number of local maxima and the probability to fail.

2.1.3. Dividing the Artery Tree into Branches

The cerebral arteries are divided into branches at bifurcations using a procedure like the region-growing technique. The cerebral arteries have been binarized since they were extracted and the voxels have a value of a signal or background. This dividing process aims to detect bifurcations and to separate branches, so that a focused voxel is extracted as a part of a branch if the value of only the voxel, not the six neighbor voxels, is a signal. Voxels of six neighborhoods of this voxel are going to become focused voxels in the next phase. The region growing proceeds throughout an artery tree (Fig. 5a). To detect bifurcations a labeling process was inserted before going to next phase. This labeling process targets only the next focused voxels. A bifurcation in an artery tree can be detected if multiple labels are given to the next focused voxels; it means that the focused voxels are split into separate connected groups (Fig. 5b).An initial seed voxel is found using raster scanning, and this dividing procedure continues until an entire artery tree is grown. Additional artery trees in the volume, if it exists, are identified using raster scanning of the volume.

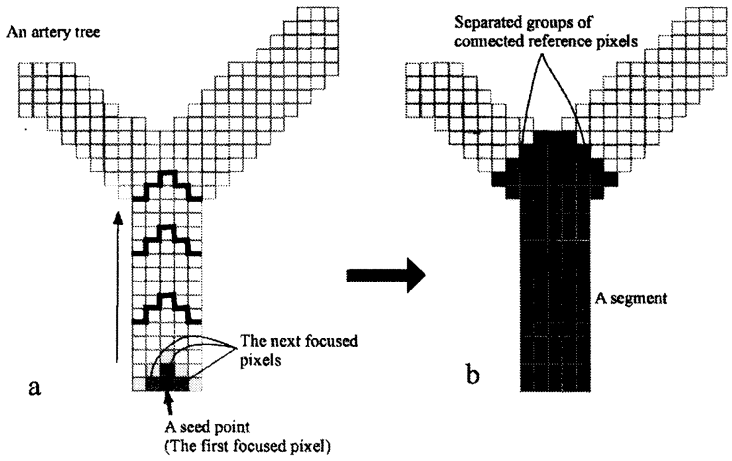

Fig. 5 Division process illustrated in 2D space.
The division spreads from a seed pixel to connected pixels (a). When the region-growing splits into two groups, the subsequent arteries are identified as other segments (b).

2.1.4. Classifying Branches into Artery Segments

The identified branches are classified as belonging to one of the cerebral artery segments. For each branch, the location of each voxel in that branch relative to the center of the CW determined above is calculated. This location is compared to the 3D segment map containing ranges for the locations of the various cerebral arteries relative to the center of CW (*see Section 2.2*). If all voxels in the branch correspond to only one vessel of the CW, the segment is labeled accordingly. If the voxels in a branch correspond to several different arteries, the segment is labeled as that artery to which the majority of the voxels correspond.

2.2. 3D Segment Map

The 3D segment map we created and used was a volume data matrix of $256 \times 256 \times 90$ (assumed voxel size: $0.5 \times 0.5 \times 1.0$ mm^3), the origin of which was located at the center the volume and was assumed to be the center of the CW. The 3D segment map had regions corresponding to 12 arteries: ACA, R- and L- ACA(A1), R- and L- MCA, R- and L- PcomA, R- and L- PCA, R- and L- ICA and BA. The voxels in each region had an individual index number of a corresponding artery segment. The segment map was divided into top and bottom blocks separated by the XY plane passing through the origin. The bottom block included the R-ICA, L-ICA and BA regions, while the top block included the others. These regions made up an essentially solid rectangular shape (Fig. 6). The 3D segment map was based on seven of the 15 cases (see *Section 2.3*). Extracted arteries, especially MCA and PCA, of the seven cases relatively spread more widely than the others.

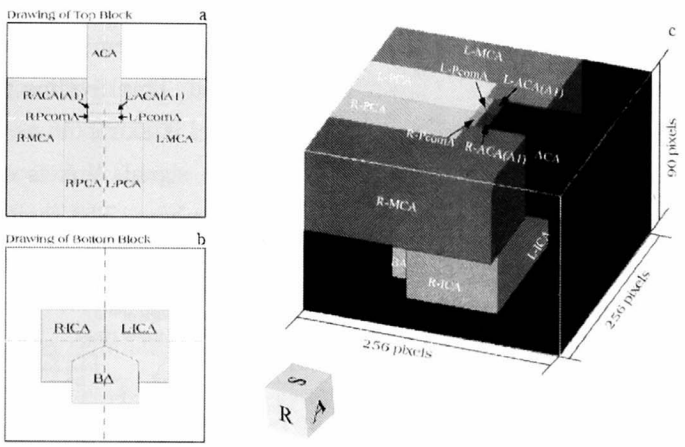

Fig. 6 3D segment map of cerebral arteries. The image (c) on the right is a volume rendered image of the 3D segment map. The two images on the left are a schematic of the top block (a) and a schematic of the bottom block (b). These areas were based on seven cases.

2.3 Materials

MRA data of the cerebral artery from 15 cases (6 men and 9 women; age range, 29–77 years old; mean, 59.1 years old) were obtained retrospectively to develop and evaluate the anatomical labeling method. All cases already had been diagnosed as cerebral aneurysm by several neuroradiologists in a hospital. In all cases, data were obtained with the routine time-of-flight MRA sequence (TR: 34–38 ms; TE: 2.8–3.5 ms; variable FA: 25 or 30° ; FOV: 130 mm) on a Signa Horizon 1.5T MRI system (GE Medical Systems, Milwaukee, WI, USA). The MRA data sets were output in the digital imaging and communication in medicine (DICOM) file format and were transferred to a computer

for analysis and processing. Each transferred data set consisted of 60 cross-sectional images of 256 × 256 × 16 bits (voxel size: 0.51 × 0.51 × 1 mm^3).

2.4. Accuracy Evaluation

Fifteen cases were examined. The labeling method was applied to seven cases used in the creation of the 3D segment map, including the five cases for the creation of the 2D and 3D templates as training data, with the other eight cases used as test data. The cerebral arteries of these cases automatically classified by the above method were compared with the manually classified cerebral arteries, which were taken as standard truth. The successful classification rates (SCR) for each of the cerebral arteries and for the entire artery tree were calculated as accuracy measures. The SCR was defined as:

$$SCR\ (\%) = \frac{N_{Successful}}{N_{True}} \times 100 \quad \cdots\cdots (1)$$

where, N_{true} is the number of voxels that comprise each of the cerebral arteries and $N_{successful}$ is the number of voxels classified correctly. Mean SCR of each artery segment of the cases was also calculated.

3. Results

The mean SCRs and standard deviations for the artery segments of the cases are shown in Table 2. The mean SCRs for major arteries, R- and L- MCA, R- and L-ICA and BA, were over 85% in the training data, and that for the entire artery tree was 84.1%. The mean SCRs for the test data were almost the same as those for the training data except for R- and L- MCA and R-PCA.

In the test data, two cases affected the mean SCRs for MCAs: one case had giant aneurysms on both R- and L-CA, and determination of the center of the CW failed in the other case. Intensity of further arteries from giant aneurysms usually becomes low because of turbulent flow. In the case

Table 2 Average numer of voxels and mean successful classification rate (SCR) for artery segments

Artery segment	Average number of voxels (voxels)	Training data (%)	Test data (%)	All cases (%)
ACA	653.1 ± 407.4	84.7 ± 9.7	80.5 ± 24.4	82.7 ± 16.1
R-ACA(A1)	231.0 ± 131.3	41.7 ± 35.4	53.4 ± 39.5	47.1 ± 36.3
L-ACA(A1)	233.7 ± 137.1	46.8 ± 44.6	45.6 ± 44.9	46.1 ± 42.2
R-MCA	1344.6 ± 802.4	97.1 ± 4.4	65.8 ± 33.1	80.4 ± 27.4
L-MCA	1271.2 ± 786.8	87.8 ± 16.5	62.2 ± 36.2	74.1 ± 30.7
R - PcomA	62.3 ± 70.0	0.0 ± 0.0	0.0 ± 0.0	0.0 ± 0.0
L-PcomA	45.7 ± 92.9	6.7 ± 7.8	0.0 ± 0.0	3.3 ± 6.1
R-PCA	609.0 ± 282.4	77.5 ± 25.5	45.2 ± 35.2	60.3 ± 34.5
L-PCA	562.6 ± 239.8	62.2 ± 28.7	71.0 ± 33.9	66.9 ± 35.4
R-ICA	4850.5 ± 2213.7	89.9 ± 7.1	91.5 ± 10.4	90.7 ± 8.5
L-ICA	4236.8 ± 1402.5	89.4 ± 15.1	91.9 ± 11.3	90.7 ± 12.6
BA	1794.5 ± 1164.7	85.9 ± 24.7	93.4 ± 7.0	89.9 ± 17.3
Entire artery tree	15892.9 ± 4734.5	84.0 ± 6.6	84.2 ± 6.5	84.1 ± 6.3

(mean value ± standard deviation)

here with giant aneurysms, most of the MCAs did not appear and the slight remaining MCAs were close to the giant aneurysms. Thus, the MCAs could not be distinguished from the aneurysms, and the SCRs for these two arteries were very low. In the case in which CW determination failed, the ACA(A1) segments descended first and ascended from around AcomA. We assumed that ACA, including ACA(A1) segment, ascended from the origin on the ICA based on the results shown in Table 1, and the 3D template was made in accordance with this profile. This difference in the arteries with the 3D template caused errors in determination of the center of the CW, although determination failed only in this one case.

Regarding R-PCA, there were two cases in the test data in which blood flow of either PCA fed mainly from PcomA affected the mean SCRs for R-PCA. In one of these two cases, about 70% of voxels in the R-PCA were classified into BA because the R-PCA fed from R-PcomA and did not branch until around the distal end after artery tree extraction and also the R-PCA appeared three or four slices below the L-PCA. In the other case, 60% of the R-PCA voxels were classified into BA. In this case the L-PCA fed from L-PcomA in contrast to the former case. The R-PCA and BA were not divided at the top of BA because these arteries were smoothly interconnected to each other.

The mean SCRs for all 15 cases were 82.7% for ACA, 47.1% for R-ACA(A1), 46.1% for L-ACA(A1), 80.4% for R-MCA, 74.1% for L-MCA, 0.0% for R-PcomA, 3.3% for L-PcomA, 60.3% for R-PCA, 66.9% for L-PCA, 90.7 for R-ICA, 90.7% for L-ICA, 89.9% for BA, and 84.1% for the entire artery tree.

Four volume rendered images of R-ICA, R-ACA(A1), ACA and R-MCA, which were extracted from MRAs according to the results obtained with our anatomical labeling method, are shown in Fig. 7 as representative results. These were the same cases as shown in Fig. 3. The SCRs for the entire artery tree for cases (a), (b), (c) and (d) were 80.1%, 70.9%, 91.3% and 92.8%, respectively. Cases (a) and (b) were included in the training data, while cases (c) and (d) were included in the test data. Fig. 7 (d) contains only a small number of voxels for the R-MCA, ACA and R-ACA(A1) arteries due to the giant aneurysms on both sides of the ICA. However, this case had the highest SCR among all cases because only easily classifiable major arteries (i.e., both sides of the ICA and PCA and the BA) were present in its original MRA.

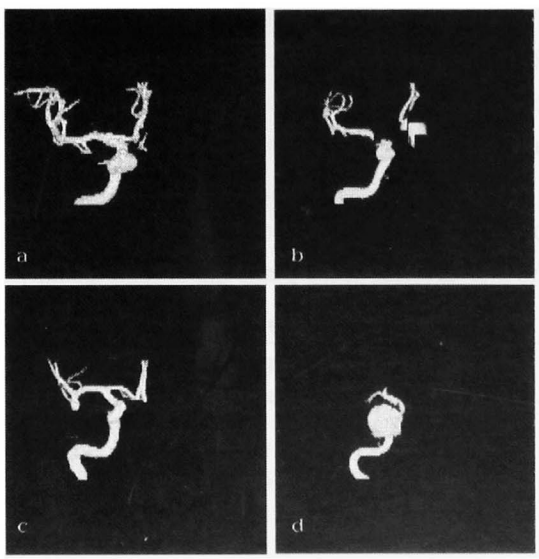

Fig. 7 Examples of isolated arteries rendered by volume rendering. The R-ICA, R-IACA(A1), ACA and R-IMCA were isolated from the MRAs according to the results. These cases are the same as those in Fig. 3. The cases shown in images (a), (b), (c), and (d) resulted in SCR of 91.3%, 80.1%, 92.8% and 70.9%, respectively.

The case in Fig. 7 (b) caused a gap in the artery tree. The SCRs of ACA, R-ACA(A1), R-MCA and

R-ICA were 71.2 %, 0.0 %, 100 % and 98.6 %, respectively. This case, and also other cases, caused a gap due to the low SCR of the R-ACA(A1) segment in this extraction. To avoid a gap, it is important to classify arteries of the CW correctly.

The volume of an artery branch appears to influence the accuracy of the labeling process. Branches with sufficient voxels can be classified correctly due to the voting system used in this labeling process, even if there are small positional errors in the detected CW center. The correlations between the SCR and the voxel count of each artery segment are shown in Fig. 8. The graph illustrates that the smaller the voxel count an artery segment had, the higher the risk of a low SCR it had. Such a tendency can be seen in Table 2. The order of mean voxel counts of the artery segments matched that of their mean SCR. In particular, both side of the PcomA and ACA(A1) had small number of voxels and these artery segments resulted in poor labeling (SCR < 50%).

The 48 arteries of all ACA, MCA and BA had relatively small voxel counts (< 2000) and SCRs for 43 of their arteries (90%) were over 50 %. These arteries spread widely, so that they were classified more easily than ACA(A1) and PcomA by the location based method. In other words, artery segments having small number of voxels and not spreading widely, like ACA(A1) and PcomA were difficult to classify by the method.

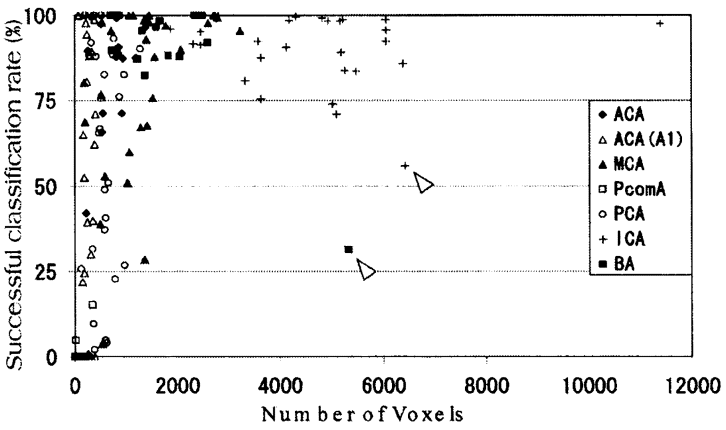

Fig. 8 Correlation of successful classification rate and voxel count for artery segment.
This graph illustrates that the smaller voxel count of an artery segment is correlated with lower SCR. The two markers (white triangles) correspond to larger voxel count and lower SCR, which occurred because of giant aneurysms.

Two outlying poor results for larger voxel counts in Fig. 8 (white triangles) corresponded to arteries located close to giant aneurysms. Giant aneurysms usually have inhomogeneous signal intensity in the MRA because of turbulent flow, and are therefore not extracted as completely as homogeneous saccular aneurysms, and the pieces are identified incorrectly as branches in the branch division process.

4. Discussion

The accuracy of this anatomical labeling scheme should be evaluated using the mean SCR for all cases because of differences in cases between the training data and the test data. Well extracted cases were chosen for the training data to create the 3D segment map, so that cases that were not easily classified probably remained in the test data. Thus, the results for only the test data would be poorer than the true performance in this scheme.

Low SCR of ACA(A1) segments caused a gap in the artery tree after the extraction with the ana-

tomical labeling results (Fig. 7b). To avoid gaps of artery trees, artery segments around the CW should be classified correctly. But the results in Table 2 indicated that arteries having a small number of voxels and not spreading widely were difficult to classify well. Regions for such arteries in the 3D segment map would be small and close to each other, so that a small positional error in the determination of the center of the CW would lead to segmentation error of these artery segments. Wide spreading and large volume artery segments, such as ICA and MCA, could cover the positional error due to the voting system. Positional error of the determination of the center of the CW was caused by aneurysms on ICAs and by the large difference of the form of the CW with the 3D template created from five cases. These deformations necessarily affected accuracy of the determination of the center of the CW with the 3D template. However, improvement of the initial extraction of cerebral arteries from MRA could provide more volume for the artery trees, of course including ACA(A1) and PcomA, and might also hold the promise of improved SCRs.

The major arteries are more important for robustness of 2D/3D registration than the small arteries because they are widely distributed and aid in global registration in 2D/3D registration. Most of the SCRs for major arteries, ACA, MCA, ICA and BA, were also over 80%. These results indicated that this anatomical labeling method should be useful for 2D/3D registration of MRA and DSA images.

Fig. 9 shows an example of 2D/3D registration results of 3D MRA data and a DSA image. The 2D/3D registration[14] was performed using the isolated MRA arteries and the DSA image. The cerebral artery tree (consisting of the R-ICA, R-MCA, R-ACA(A1) and ACA) in the 3D volume was isolated using the results obtained with the anatomical labeling scheme. The SCR was 89.7% for the entire artery tree, which was close to the average SCR. The pair of images indicated that the MRA arteries were well registered with the DSA image.

Further development of the proposed method will improve its usefulness. Broken artery trees do not necessarily result in registration failure, although it appears that poor registration occurs more frequently for arteries with low SCRs. Further investigations into the robustness of the 2D/3D registration method combined with this anatomical labeling method are currently underway in our laboratory.

Fig. 9 An example of paired 3D isolated artery and a DSA image. Image (a) shows a DSA image obtained by internal carotid arteriography. Image (b) shows volume rendered 3D data of the arteries isolated from MRA according to our labeling results. The 3D arteries were aligned using our 2D/3D registration technique. The case resulted in an SCR of 89.7%.

We also think that the anatomical labeling technique has the potential to facilitate reporting locations of disease candidates in combination with MRA-based CAD systems for cerebral aneurysms[24,25]. But, currently, accuracy of this method must be improved, especially for ACA(A1)

segment and PcomA, because cerebral aneurysms often occur on the CW.

5. Conclusions

An automatic anatomical labeling method for cerebral arteries in MRA has been developed. This method gave the mean SCR of 84.1% for the entire artery tree, and the 2D/3D registration combined with the anatomical labeling method resulted in an SCR of 89.7 % near the mean SCR. Thus, this anatomical labeling method is useful for 2D/3D registration. In addition, it is expected that improved extraction of small arteries would raise the accuracy of the method.

Acknowledgements

We would like to thank Dr. Kenneth R. Hoffmann, The Toshiba Stroke Research Center, State University of New York at Buffalo, for helpful advice and suggestions. This work is supported by a grant-in-aid for young scientists (B) (KAKENHI 15790656) of The Ministry of Education, Culture, Sports, Science and Technology of Japan.

References

1) Penney GP, Weese J, Little JA, et al: A comparison of similarity measures for use in 2-D-3-D medical image registration. IEEE Trans. Med. Imag. 17(4): 586－595, 1998
2) Penney GP, Batchelor PG, Hill DL, et al: Validation of a two- to three-dimensional registration algorithm for aligning preoperative CT images and intraoperative fluoroscopy images. Med. Phys.28(6): 1024－1032, 2001
3) Nakajima Y, Tamura Y, Sato Y, et al: Preoperative Analysis of Optimal Imaging Orientation in Fluoroscopy for Voxel-Based 2-D/3-D Registration. in proc MICCAI2002: 485－492, 2002
4) Tomaevie D, Likar B, Pernus F: "Gold Standard" 2D/3D Registration of X-Ray to CT and MR Images. in proc. MICCAI2002: 461－468, 2002
5) Imamura H, Ida N, Sugimoto N, et al: Registration of Preoperative CTA and Intraoperative Fluoroscopic Images for Assisting Aortic Stent Grafting. In Proc. MICCAI2002: 477－484, 2002
6) Wein W, R¨oper B, Navab N: 2D/3D Registration Based on Volume Gradients. In Proc. SPIE Medical Imaging 5747: 144－150, 2005
7) Rohlfing T and Maurer Jr. CR: A Novel Image Similarity Measure for Registration of 3-D MR Images and X-Ray Projection Images. in proc.MICCAI2002: 469－476, 2002
8) Feldmar J, Ayache N, Betting F: 3D-2D projective registration of free-form curves and surfaces. Computer vision and image understanding 65(3): 403－424, 1997
9) Kita Y, Wilson DL, Noble JA: Real-time registration of 3D cerebral vessels to X-ray angiograms. In Proc. MICCAI'98: 1125－1133, 1998
10) Kerrien E, Berger MO, Maurincomme E, et al: Fully automatic 3D/2D subtracted angiography registration. In Proc. MICCAI'99: 664－671, 1999
11) McLaughlin RA, Hipwell JH, Penney GP, et al: Intensity-based Registration versus Feature-

based Registration for Neurointerventions. Medical image understanding and analysis 2001: 69-72, 2001

12) Hipwell JH, Penney GP, Cox TC, et al: 2D-3D Intensity Based Registration of DSA and MRA -Comparison of Similarity Measures. In Proc. MICCAI2002: 501-508, 2002

13) Vermandel M, Kulik C, Gauvrit JY, et al: Registration and matching of projection imaging and tomographic imaging. Application to X-rays angiographies and magnetic resonance angiographies. In Proc.CARS2002: 419-424, 2002

14) Takemura A, Harauchi H, Suzuki M, et al: An algorithm for mapping the catheter tip position on a fluorograph to the three-dimensional position in magnetic resonance angiography volume data. Physics in Medicine and Biology 48: 2697-2711, 2003

15) Hipwell JH, Penney GP, McLaughlin RA, et al: Intensity-based 2-D-3-D registration of cerebral angiograms. IEEE Trans. Med. Imag. 22(11): 1417-1426, 2003

16) Summers PE, Bhalerao AH, Hawkes DJ: Multiresolution, model-based segmentation of MR angiograms. J Magn Reson Imag. 7(6): 950-957, 1997

17) Sato Y, Nakajima S, Shiraga N, et al: Three-dimensional multi-scale line filter for segmentation and visualization of curvilinear structures in medical images. Medical Image Analysis 2(2): 143-168, 1998

18) Wilson DL, Noble JA: An adaptive segmentation algorithm for extracting arteries and aneurysms from time-of-flight MRA data. IEEE Trans. Med. Imag. 18(10): 938-945, 1999

19) Bullitt E, Aylward S, Smith K, et al: Symbolic description of intracerebral vessels segmented from magnetic resonance angiograms and evaluation by comparison with X-ray angiograms. Medical Image Analysis 5(2): 157-169, 2001

20) Lorigo LM, Faugeras OD, Grimson WE, et al: CURVES: curve evolution for vessel segmentation. Medical Image Analysis 5(3): 195-206, 2001

21) Sabry MM, Sites CB, Farag AA, et al: A fast automatic method for 3D volume segmentation of the human cerebrovascular. In. Proc. CARS2002: 382-387, 2002

22) Chen J, Amini AA: Quantifying 3-D vascular structures in MRA images using hybrid PDE and geometric deformable models. IEEE Trans. Med. Imag, 23(10): 1251-1262, 2004

23) Press WH, Teukolsky SA, Vetterling WT, Flannery BP: Minimization or Maximization of Functions. In: Numerical Recipes in C++ 2nd ed., PP398-460, 2003, Cambridge University Press: New York

24) Suzuki K, Armato SG 3rd, Li F, et al: Massive training artificial neural network (MATANN) for reduction of false positive in computerized detection of lung nodules in low-dose computed tomography. Med. Phys. 30(7): 1602-1617, 2003

25) Arimura H, Li Q, Korogi Y, et al: Automated computerized scheme for detection of unruptured intracranial aneurysms in three-dimensional magnetic resonance angiography. Acad Radiol. 11(10): 1093-1104, 2004